Cardiovascular Research (2014) **101**, 411–422
doi:10.1093/cvr/cvt338

Reversible and irreversible differentiation of cardiac fibroblasts

Ronald B. Driesen[1]*, Chandan K. Nagaraju[1], Joëlle Abi-Char[1], Tamara Coenen[2], Paul J. Lijnen[2], Robert H. Fagard[2], Karin R. Sipido[1†], and Victor V. Petrov[2†]

[1]Department of Cardiovascular Diseases, Division of Experimental Cardiology, University of Leuven, KU Leuven, Campus Gasthuisberg O/N1 Box 704, Herestraat 49, Leuven B-3000, Belgium; and [2]Department of Cardiovascular Medicine, Division of Hypertension, University of Leuven, KU Leuven, Leuven, Belgium

Received 22 August 2012; revised 16 December 2013; accepted 18 December 2013; online publish-ahead-of-print 23 December 2013

Time for primary review: 50 days

Aims Differentiation of cardiac fibroblasts (Fbs) into myofibroblasts (MyoFbs) is responsible for connective tissue build-up in myocardial remodelling. We examined MyoFb differentiation and reversibility.

Methods and results Adult rat cardiac Fbs were cultured on a plastic substratum providing mechanical stress, with conditions to obtain different levels of Fb differentiation. Fb spontaneously differentiated to proliferating MyoFb (p-MyoFb) with stress fibre formation decorated with alpha-smooth muscle actin (α-SMA). Transforming growth factor-β1 (TGF-β1) promoted differentiation into α-SMA-positive MyoFb showing near the absence of proliferation, i.e. non-p-MyoFb. SD-208, a TGF-β-receptor-I (TGF-β-RI) kinase blocker, inhibited p-MyoFb differentiation as shown by stress fibre absence, low α-SMA expression, and high proliferation levels. Fb seeded in collagen matrices induced no contraction, whereas p-MyoFb and non-p-MyoFb induced 2.5- and four-fold contraction. Fb produced little collagen but high levels of interleukin-10. Non-p-MyoFb had high collagen production and high monocyte chemoattractant protein-1 and tissue inhibitor of metalloproteinases-1 levels. Transcriptome analysis indicated differential activation of gene networks related to differentiation of MyoFb (e.g. paxilin and PAK) and reduced proliferation of non-p-MyoFb (e.g. cyclins and cell cycle regulation). Dedifferentiation of p-MyoFb with stress fibre de-polymerization, but not of non-p-MyoFb, was induced by SD-208 despite maintained stress. Stress fibre de-polymerization could also be induced by mechanical strain release in p-MyoFb and non-p-MyoFb (2-day cultures in unrestrained 3-D collagen matrices). Only p-MyoFb showed true dedifferentiation after long-term 3-D cultures.

Conclusions Fb, p-MyoFb, and non-p-MyoFb have a distinct gene expression, ultrastructural, and functional profile. Both reduction in mechanical strain and TGF-β-RI kinase inhibition can reverse p-MyoFb differentiation but not non-p-MyoFb.

Keywords Cardiac fibroblast • Myofibroblast • Dedifferentiation

1. Introduction

Fibroblasts (Fbs) are the most numerous cell type in the heart,[1] whereas myofibroblasts (MyoFbs) appear in pathological conditions. Two factors are responsible for Fb differentiation, i.e. transforming growth factor-β1 (TGF-β1) produced by inflammatory cells at the onset of pathology[2] and mechanical stress.[3] Differentiation of Fb into MyoFb is responsible for remodelling processes, such as collagen deposition, matrix remodelling,[4] and scar formation,[5] and is implicated in enhanced production of angiotensin by angiotensin-converting enzyme.[6] Both inflammation and fibrosis were directly correlated to diastolic dysfunction in heart failure with a preserved ejection fraction.[7] Fb differentiation consists of two steps: (i) differentiation to proto-MyoFb that shows G-actin polymerization into F-actin stress fibres and (ii) further differentiation into MyoFb in which stress fibres are decorated with alpha-smooth muscle actin (α-SMA).[8] Polymerization of F-actin stress fibres prevents sequestration of myocardin-related transcription factors (MRTFs) in the cytosol by G-actin. Consequently, MRTFs translocate to the nucleus where they support activation of α-SMA expression.[9]

When Fbs are isolated from tissue and grown on a stiff plastic substratum, they eventually develop strong cell tension that induces TGF-β1 production.[10] Moreover, TGF-β1 is constitutively present in

* Corresponding author. Tel: +32 16 330179; fax: +32 16 345844. Email: ronald.driesen@med.kuleuven.be

† These authors contributed equally.

© The Author 2013. Published by Oxford University Press on behalf of the European Society of Cardiology.
This is an Open Access article distributed under the terms of the Creative Commons Attribution Non-Commercial License (http://creativecommons.org/licenses/by-nc/3.0/), which permits non-commercial re-use, distribution, and reproduction in any medium, provided the original work is properly cited. For commercial re-use, please contact journals.permissions@oup.com

serum-enriched culture media.[11] These factors will lead to spontaneous Fb differentiation confounding studies of fibroblast–myocyte interactions in 2-D cultures[12,13] and complicating the study of non-activated Fb.

The process of MyoFb dedifferentiation has been well characterized in non-cardiac cells,[14,15] but whether the cardiac MyoFb phenotype is reversible remains under debate, possibly related to a spectrum of MyoFb phenotypes. Reversing MyoFb to Fb might hold excellent promise as a new therapeutic target in attenuating fibrosis and diastolic dysfunction and could potentially be achieved. Indeed, loss of strain in non-cardiac MyoFb reduces α-SMA expression[3] and decreases collagen Type I production,[16] while a recent study demonstrated that suppression of α-SMA reduced arrhythmogenic effects of cardiac MyoFb co-cultured with cardiomyocytes.[17] Inhibition of TGF-β1-induced SMAD3 up-regulation could be another pathway for restricting MyoFb activity.[18]

The purpose of the present study was to distinguish the different Fb cell types that can be derived from the heart, the mechanisms driving differentiation and the distinct capacities for dedifferentiation of these different Fb cells. We develop tools to obtain highly enriched, near-pure populations of different cardiac Fb phenotypes in 2-D cultures. We characterize the phenotypical plasticity of non-activated cardiac Fb and differentiated MyoFb at a structural, functional, and molecular level. Furthermore, we seed different types of MyoFbs into 3-D collagen matrices (3-DCMs) to identify the role of mechanical stress and growth factors in a more physiological environment and to further study the potential for dedifferentiation of MyoFb.

2. Methods

The investigation conforms with the Guide for the Care and Use of Laboratory Animals published by the US National Institutes of Health (NIH Publication, 8th Edition, 2011). The research protocol is approved by the Ethical Committee for Animal Experiments of the KU Leuven, Belgium. Detailed information on all experimental protocols and data acquisition can be found in Supplementary material online.

2.1 Animal procedures and cell cultures

Cardiac left ventricular Fbs were enzymatically isolated from hearts of male Wistar rats (*Rattus norvegicus*, 7–8 weeks old) as previously described.[19] After heparin injection (625 U/100 g), deep anaesthesia was induced with pentobarbital (50 mg/100 g body weight). The heart was removed and washed in Joklik's medium. The aorta was cannulated and mounted on a Langendorff perfusion system. After enzymatic digestion, the pellet was resuspended in DMEM (Gibco, Invitrogen, Belgium) supplemented with 10% foetal bovine serum (FB, Gibco, Invitrogen, Belgium), and 1% of penicillin/streptomycin solution and seeded in an 75 cm^2 tissue culture flask. After second passage, Fbs were seeded at a density of 2600 cells/cm^2 and cultured in DMEM medium with 10% FB. To test differentiation and dedifferentiation pathways, we used SD-208 (3 μmol/L; Sigma-Aldrich, Belgium), a specific TGF-β-receptor-I (TGF-β-RI) kinase inhibitor, Y-27632, a Rho-kinase inhibitor (10 μmol/L, CalBiochem 688001, Belgium), recombinant human TGF-β1 (400 pmol/L; PeproTech, USA), and a combination of SD-208 (3 μmol/L) and TGF-β1 (400 pmol/L). To evaluate proliferation capacity, 24-well culture plates (Costar, Corning Incorporated, USA) were seeded with 5000 cells per well, with or without treatment. After 12 days in culture, cells were counted in a Bürker counting chamber. All the experiments comparing cell differentiation and dedifferentiation were a paired study design, i.e. the different treatments were applied to cultures from the same heart. Experiments were repeated ≥3 animals.

2.2 Reverse transcription and semi-quantitative PCR

Total RNA was isolated from different cell cultures using TRIzol reagent (Invitrogen) and purified on RNeasy Mini Kit columns (Qiagen). Primers used for qRT-PCR analysis are shown in Supplementary material online, *Table S1*. qRT-PCR was performed on a 7500 Fast Real-Time PCR machine using the SYBRGreen master mix (Applied Biosystems, Belgium). The relative gene expression was calculated by comparing cycle times for target PCR using the following equation: relative gene expression = $2^{-(\Delta C_{tsample} - \Delta C_{tcontrol})}$. Values are normalized to GAPDH expression levels.

2.3 Sircol collagen assay and cytokine array

Total collagen production was determined using the Sircol Collagen Assay kit (Biocolor, County Antrim, UK). Cytokine secretion was measured in conditioned media using the Quantibody Rat Cytokine Array 2 (RayBiotech, Norcross, USA). Simultaneous quantification of 10 cytokines was performed on a GenePix 4000B Microarray scanner. Collagen and cytokine measurements were analysed according to the manufacturer's instructions.

2.4 Microarray transcriptome analysis

RNA concentration and purity were determined spectrophotometrically using the Nanodrop ND-1000 (Nanodrop Technologies), and RNA integrity was assessed using a Bioanalyser 2100 (Agilent). cDNA and hybridization controls (Affymetrix) were hybridized on an Affymetrix GeneChip® Rat Gene 2.0 ST array. To assess raw probe signal intensities, chips were scanned using a GeneChip® scanner 3000 (Affymetrix). Biological pathway and network analysis were analysed using an Ingenuity Pathway Analysis software (IPA). Raw data files are available on GEO (accession number GSE51824).

2.5 Western blot analysis

Whole cell lysates were prepared using the Cell Lytic M Cell lysis reagent (Sigma, Belgium), and total protein was quantified using the Pierce BCA Protein Assay Kit (Thermo Scientific, Belgium). Equal samples were loaded and separated by electrophoresis. Proteins were transferred onto a membrane (Invitrogen) and incubated with α-SMA (Sigma) or β-tubulin antibody (Abcam, Belgium). Blots were developed and captured on X-ray film (Super RX FujiFllm). α-SMA protein expression levels were assessed and normalized to β-tubulin using an ImageJ (National Institutes of Health, http://rsb.info.nih.gov/ij/, USA) software.

2.6 Three-dimensional collagen matrices

The ability of Fb and MyoFb to contract extracellular matrix was evaluated with unrestrained 3-DCM and was prepared from rat tail collagen. The volume of the 3-DCM was estimated by measurement of the ^3H_2O distribution between the 3-DCM and medium. Toroid-shaped restrained 3-DCMs were prepared by mixing Fb cells with collagen Type I and serum-containing culture medium (2× DMEM, 20% horse serum, and 1% penicillin and streptomycin). Collagen rings were cultured during 14 days.

2.7 Immunostaining of isolated cells

Immunostaining was performed on cultured cells and stained for α-SMA (Sigma) or vinculin (Santa Cruz, Germany). Immunofluorescence staining was used to evaluate the presence of stress fibres using α-SMA and Rhodamin-Phalloidin staining (Invitrogen, Molecular Probes, Belgium). Unrestrained 3-DCMs were double-stained with α-SMA and Rhodamin-Phalloidin actin. Six randomly chosen fields were analysed for each study. Paraffin sections of restrained 3-DCMs were immunostained using α-SMA, and cells were analysed for positivity in a 500 μm × 500 μm area of each section. Image analysis was performed using the Axiovision, LSM 510, and ImageJ software.

2.8 Statistical analysis

Values are expressed as mean ± SEM. All the data were obtained in cell cultures from primary isolation of 3–6 animals as indicated in the figure legends. All comparisons of Fb phenotypes were performed in matched cultures, i.e. derived from the primary cell isolation; values in the figure legends refer to the number of animals from which primary cells were isolated. The statistical methods used are repeated-measures analysis of variance, Student's two-tailed test for unpaired data, and one-way analysis of variance with Bonferroni's multiple comparison tests. Normalized intensity values from microarray analysis were compared with the limma package. Microarray *P*-values were corrected for multiple testing with Benjamin-Hochberg and core analysis was performed with a log ratio of 1. A *P*-value of <0.05 is considered significant.

3. Results

3.1 Two-dimensional cultures on a stiff substrate induces different populations of Fb cells

Fbs spontaneously differentiate into MyoFbs (*Figure 1A*) in 2-D cultures in the presence of serum. MyoFbs are spread and have stress fibres (*Figure 1A*,a) decorated with α-SMA (*Figure 1A*,b) and prominent vinculin staining (*Figure 1A*,c). As these MyoFbs actively proliferate (*Figure 1E*), they are referred to as proliferative MyoFb (p-MyoFb).[19] After 4 days, p-MyoFbs make up 76 ± 4% of the total cell population (*Figure 1F*). In the presence of TGF-β1 (400 pmol/L), differentiation is enhanced (*Figure 1C*) with a remarkable increase in MyoFb size, in the stress fibre network (*Figure 1C*,a) decorated with α-SMA (*Figure 1C*,b), and expression of vinculin (*Figure 1C*,c). TGF-β1-induced differentiation of p-MyoFb is associated with a significant increase in the percentage of α-SMA-positive MyoFb (96 ± 1%, $P < 0.05$, *Figure 1F*), α-SMA protein expression (*Figure 1G*), and loss of MyoFb proliferative capacity (*Figure 1E*). These results indicate that studying genuine Fb features in 2-D cultures with serum is confounded by spontaneous MyoFb differentiation.

As TGF-β1 is the major growth factor responsible for MyoFb differentiation,[20] we tested the block of TGF-β-RI signalling with SD-208 (3 μmol/L) (*Figure 1B*). Addition of SD-208 results in a remarkable decrease in cell size, the complete absence of stress fibres (*Figure 1B*,a) as well as α-SMA (*Figure 1B*,b), and low intensity of vinculin staining (*Figure 1B*,c). Proliferative capacity is enhanced three-fold when compared with spontaneous differentiated p-MyoFb (*Figure 1E*). The percentages of α-SMA-positive MyoFb and α-SMA protein expression are strikingly reduced (*Figure 1F* and *G*). SD-208 prevents Fb differentiation even in the presence of TGF-β1. Fbs cultured in these conditions show no stress fibres (*Figure 1D*,a), diffuse cytoplasmic α-SMA (*Figure 1D*,b), and strongly reduced vinculin staining (*Figure 1D*,c). The reduced level of differentiation is quantified as a large reduction in the percentage of α-SMA-positive cells (*Figure 1F*). The effect of SD-208 is reversible, because TGF-β1 supplementation for 4 days to the culture medium after removal of SD-208 restores MyoFb differentiation (data not shown).

TGF-β1 is known to activate Rho-GTPase and ROCK,[21] which promotes G-actin polymerization into F-actin stress fibres. Inhibition of ROCK for 4 days with Y-27632 decreases α-SMA protein expression when compared with untreated cultures of p-MyoFb (*Figure 1G*). However, the effect of TGF-β-RI blockade on α-SMA expression was much more efficient compared with p-MyoFb (*Figure 1G*). These data confirm that ROCK-dependent Fb differentiation is a pathway of TGF-β1-induced differentiation.[22]

Both TGF-β1 and ROCK signalling pathways promote nuclear transfer of MRTF-A/B, activators of α-SMA expression.[9] We studied whether MRTF-A/B mRNA expression levels were differentially regulated in different Fb phenotypes. p-MyoFb shows high levels of MRTF-A expression, whereas SD-208-treated Fb demonstrates low expression (*Figure 1H*). With TGF-β1-induced differentiation of non-p-MyoFb, MRTF-A expression is significantly lower than in p-MyoFb and at the same level as SD-208-treated Fb. MRTF-B expression levels show a similar tendency.

3.2 Phenotypes of MyoFb cells in unrestrained 3-DCM

In unrestrained 3-DCMs, we examined how low mechanical strain and a more physiological 3-D environment affected the fibroblastic phenotypes obtained in 2-D cultures. Cultures were studied in the absence of growth factors (no serum). Starting from SD-208-treated Fb populations, all fibroblastic cells are round-shaped after embedding (*Figure 2A*,a). One day later, 19% change their shape into dendritic cells with multiple long and thin extensions (*Figure 2A*,b). 16% of the cells become elongated with stress fibres (*Figure 2B*). Dendritic cells are distributed in the centre of the matrix, while the elongated phenotype is more frequent at the edges of the matrix. Dendritic Fbs do not contain stress fibres and show cortical F-actin, whereas elongated cells show stress fibres (*Figure 2A*,d). By Day 2, dendritic cells account for 34% and elongated cells 27% of the cell population (*Figure 2B*).

In contrast to Fb, the majority of p-MyoFb spread out quickly. One day after embedding 62% and 10% of the cell population acquire stress fibre-positive elongated and dendritic phenotypes, respectively (*Figure 2A*,c). After 2 days, these fractions remain comparable (*Figure 2B*). Non-p-MyoFb spread out even faster than p-MyoFb. Even 1 day after embedding 86% of the total population consists of spread-out cells, stress fibre-positive dendritic (16%), and elongated cells (65%) (*Figure 2B*). The number of elongated MyoFb slightly increases further to 77% at Day 2 of culture (*Figure 2B*).

We also examined the presence of α-SMA (see Supplementary material online, *Figure S1*). Surprisingly, on Day 1, all dendritic and elongated Fbs originating from SD-208 pre-treated 2D cultures show staining for α-SMA that was, however, diffuse and not organized (see Supplementary material online, *Figure S1A*). Even in elongated cells with stress fibres, α-SMA is not incorporated into these stress fibres (see Supplementary material online, *Figure S1B*), indicating these cells are proto-MyoFb.

Contrary to progenies of Fb, dendritic and elongated progenies of p-MyoFb (see Supplementary material online, *Figure S1C–E*) and non-p-MyoFb (*Figure 1F–H*) show stress fibres that are decorated with α-SMA. Serum promotes differentiation of SD-208 pre-treated dendritic Fb into elongated cells with stress fibres but without α-SMA incorporation (data not shown).

All fibroblastic phenotypes (*Figures 2A*, *C*, and *E*, and Supplementary material online, *Video S1*) and networks (*Figure 3G* and Supplementary material online, *Video S2*) in 3-DCM are flat as demonstrated by the YX and ZX plane of orientation. F-actin in dendritic extensions of Fb often has a punctuated structure and is split into discrete grains at the end of the extensions (see Supplementary material online, *Figure S2B*). The area of grains in p-MyoFb and non-p-MyoFb is larger than that in Fb (see Supplementary material online, *Figure S2D*) and seem to

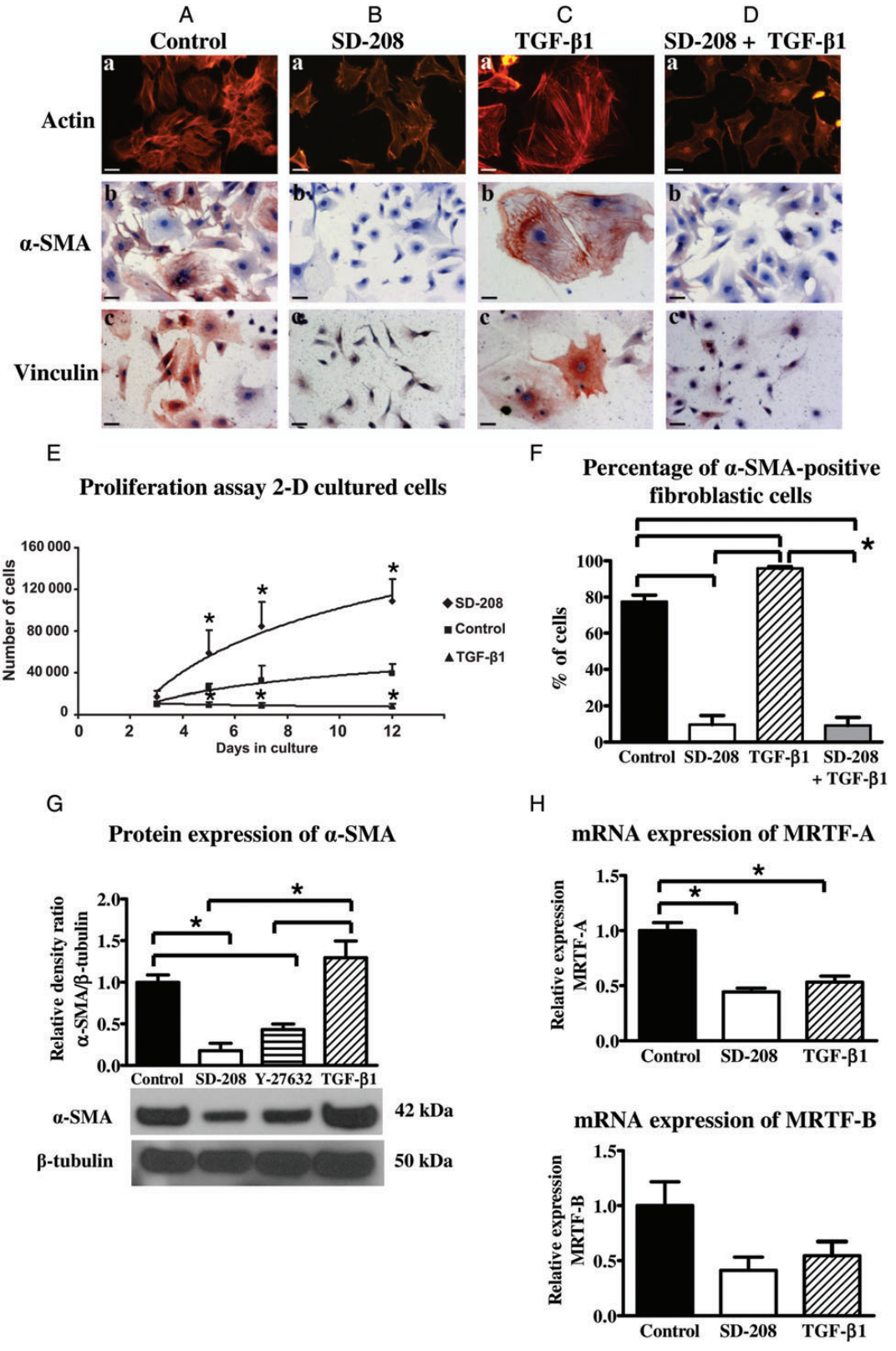

Figure 1 Differentiation of Fb cells in 2-D cultures and MRTF-A/B expression. (*A*–*D*) Different phenotypes, cells are stained for F-actin (a), α-SMA (b), and vinculin (c); scale bars represent 40 μm. (*A*) Spontaneously differentiation to p-MyoFb during 4 days in standard culture medium. (*B*) Treatment with SD-208 (3 μmol/L), an inhibitor for TGF-β-RI kinase, for 4 days maintains the Fb phenotype. (*C*) Treatment with TGF-β1 (400 pmol/L) for 6 days induces non-p-MyoFb. (*D*) Fb cultures are treated simultaneous with SD-208 (3 μmol/L) and TGF-β1 (400 pmol/L) for 4 days. (*E*) Proliferative capacity of cells after 12 days in culture. (*F*) Quantification of immunostained α-SMA-positive cells in different Fb cultures. Western blotting (*G*) of α-SMA in p-MyoFb, SD-208-treated Fb, and Y-27632-treated Fb (4-day-old cultures) and in TGF-β1-treated MyoFb (6-day-old cultures). (*H*) mRNA expression of MRTF-A/B in different Fb phenotypes. *$P < 0.05$ vs. p-MyoFb (control) or non-p-MyoFb ($N = 5$).

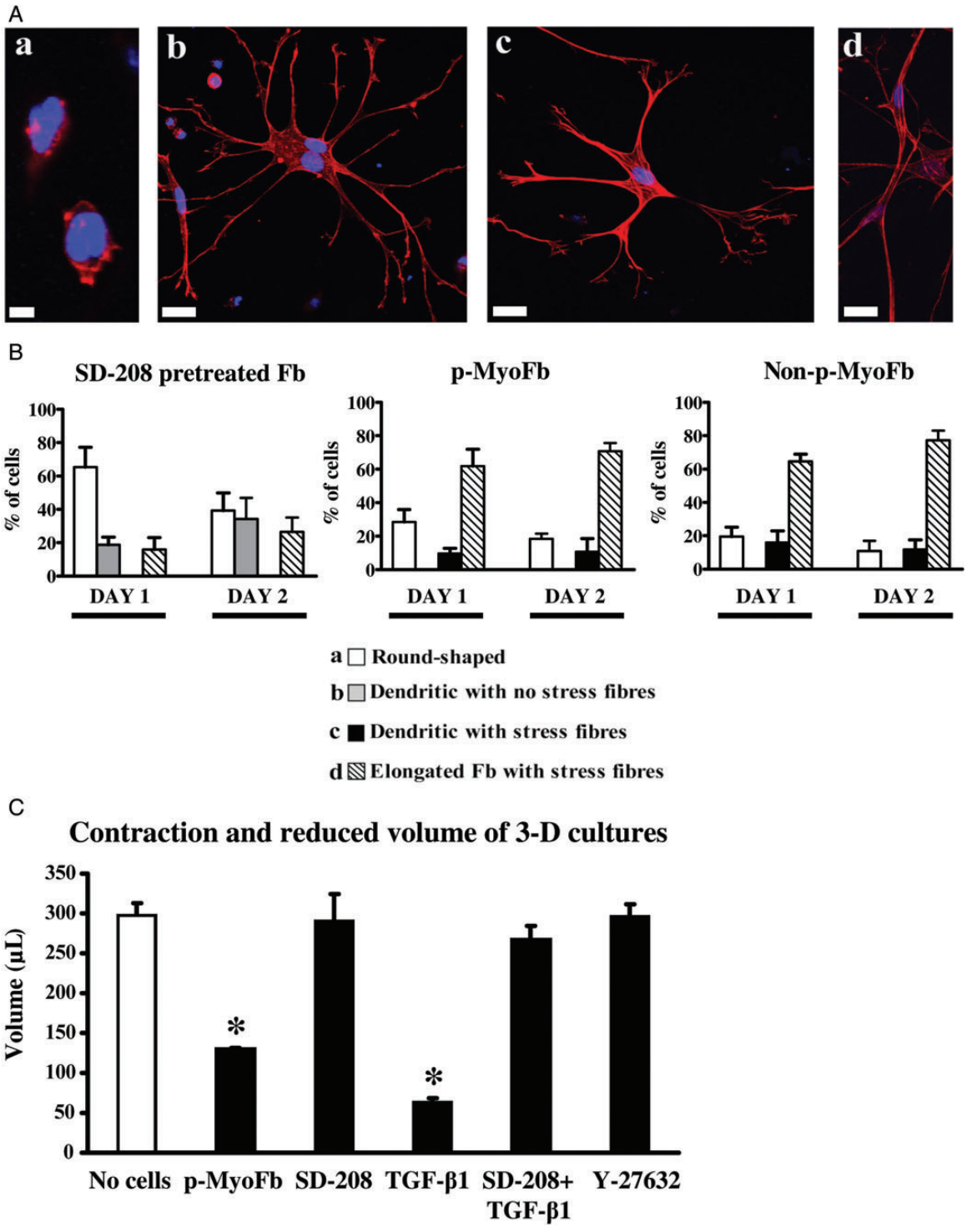

Figure 2 Structural adaptations of Fb cells in unrestrained 3-DCMs. (*A*) Fb phenotypes; Rhodamin-Phalloidin (red) marks stress fibres; nuclei stained with DAPI (blue); scale bars represent 10 µm. (a) Round phenotype, (b) dendritic phenotype without stress fibres, (c) dendritic phenotype with stress fibres, and (d)elongated phenotype with stress fibres. (*B*) Quantification of the cell fractions with specific phenotypes in the absence of serum. Fbs in 3-D cultures without mechanical strain and serum acquire a dendritic phenotype without stress fibres. p-MyoFb and non-p-MyoFb acquire an elongated phenotype with stress fibres. (*C*) Contraction of unrestrained 3-DCM by Fb cells. Volume of unrestrained 3-DCM after 3-day cultures. 3-DCMs were populated with: p-MyoFb; Fb pre-treated in 2-D cultures with SD-208 (3 µmol/L); non-p-MyoFb pre-treated with TGF-β1 (400 pmol/L); Fb pre-treated with SD-208 (3 µmol) and TGF-β1(400 pmol/L); Fb pre-treated with Y-27632 (10 µmol/L). No cells represent control 3-DCM without cells. *$P < 0.05$ vs. 3-DCM without cells ($N = 3$). Scale bars represent 5 (*A*a) and 20 (*A*b, c, and d) µm.

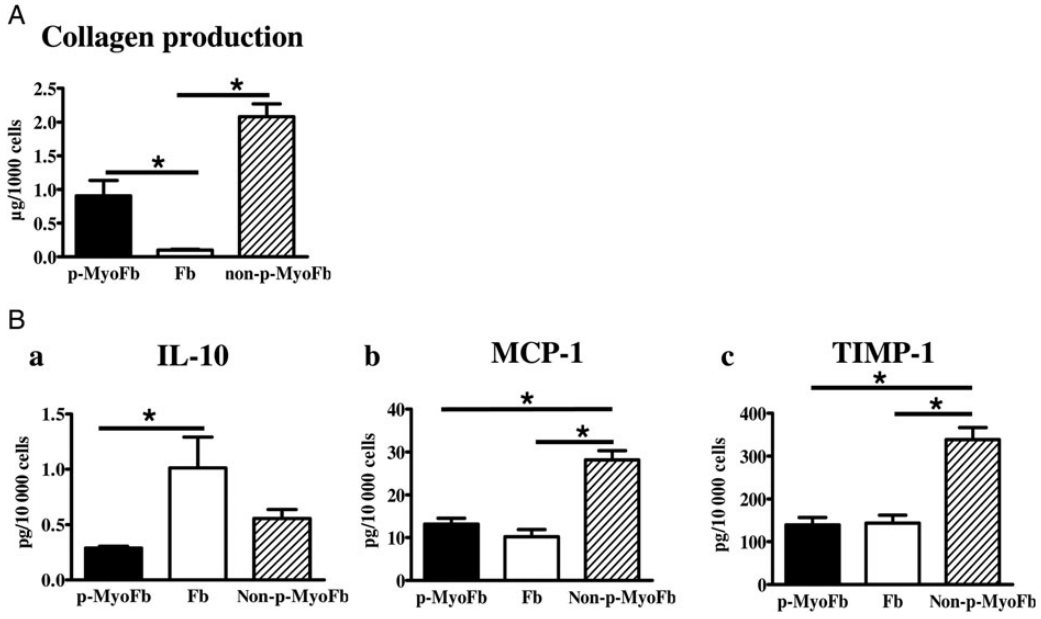

Figure 3 Collagen production and cytokine secretion in Fb cells. (*A*) Intracellular collagen production in Fb, p-MyoFb, and non-p-MyoFb ($N = 5$). (*B*) Release of IL-10 (a) MCP-1 (b), TIMP-1, and (c) in conditioned media of different Fb phenotypes ($N = 6$). *$P < 0.05$ vs. p-MyoFb or non-p-MyoFb.

belong to focal adhesions that in p-MyoFb and non-p-MyoFb are connected with stress fibres (see Supplementary material online, *Figure S2F*).

3.3 Contraction of unrestrained matrices is dependent on Fb differentiation

Contraction of unrestrained 3-DCM by fibroblastic cells is highly dependent on stress fibre formation, association of stress fibres with α-SMA, and linkage of cells into a cell network.[23] Our data show that 3-D cultures of SD-208 pre-treated Fbs which predominantly consist of stress fibre-negative dendritic Fb in the centre are not capable of contracting 3-DCM in the absence of serum (*Figure 2C*). SD-208 pre-treated Fbs have limited intercellular contacts and an absence of a cellular network (see Supplementary material online, *Figures S3* and *S4*). Pre-treatment of Fb in 2-D cultures with Y-27632 likewise inhibits 3-DCM contraction (*Figure 2C*). In contrast to SD-208 pre-treated Fb, progenies of p-MyoFb markedly compact the volume of 3-DCM by 2.5-fold compared with 3-DCM without cells. Matrices populated with non-p-MyoFb contract even more strongly by four-fold (*Figure 2C*). Three-dimensional cultures with p-MyoFb and non-p-MyoFb show intercellular contacts and a dense cellular network at the centre and periphery compared with 3-DCM populated with SD-208-treated cells (see Supplementary material online, *Figures S3* and *S4*). Serum even promotes the formation of cellular networks (see Supplementary material online, *Figures S3* and *S4*). These data indicate that 3-DCM contraction is only executed by cells, which contain stress fibres and are organized into a network.

3.4 Different levels of Fb differentiation are associated with different collagen and cytokine production

Fb differentiation is associated with increased collagen production.[24] While Fbs show low levels of collagen synthesis, collagen production is 7.4-fold higher in p-MyoFb and 17.2-fold in non-p-MyoFb compared with Fb ($P < 0.05$; *Figure 3A*).

As differentiation of Fb is accompanied by increased secretion of inflammatory cytokines,[25] we evaluated the basal secretion of cytokines in the culture medium by the different Fb phenotypes. We used a protein array in which different cytokines were quantified simultaneously. Six cytokines are below the detection limit (IL-1β, IL-6, TNF-α, IFNγ, Leptin, and L-selectin), but a number shows strong differential regulation. Fbs secrete high levels of the anti-inflammatory cytokine interleukin-10 (IL-10), whereas non-p-MyoFb release high amounts of the inflammatory cytokines monocyte chemoattractant protein-1 (MCP-1) and tissue inhibitor of metalloproteinases-1 (TIMP-1) (*Figure 3B*). The latter cytokines are both involved in extracellular matrix remodelling. p-MyoFbs show no significant secretion of these two cytokines secreted by the non-p-MyoFb or of the anti-inflammatory cytokine IL-10 produced by Fb.

3.5 Distinct expression profiles in different Fb phenotypes

We examined gene expression profiles in the different Fb phenotypes using a transcriptome analysis. A high number of differentially expressed genes is found between Fb and p-MyoFb ($n = 499$) and even more between Fb and non-p-MyoFb ($n = 1102$). Comparison between p-MyoFb and non-p-MyoFb shows a lower number of differentially expressed genes ($n = 117$). The top 100 of differentially expressed genes from the three phenotype comparisons are represented as heatmaps 1 (Fb vs. p-MyoFb), 2 (Fb vs. non-p-MyoFb), and 3 (non-p-MyoFb vs. p-MyoFb) in *Figure 4A*. Lists of the top 30 of differentially expressed genes are included as Supplementary material online, *Table S2A–F*.

Given the large number of differentially expressed genes, rather than focusing on selected genes, we aimed to identify gene networks, by analysing the data using the IPA Ingenuity software. As illustrated in *Figure 4B*, networks implicated in Fb to MyFb differentiation include 'hepatic

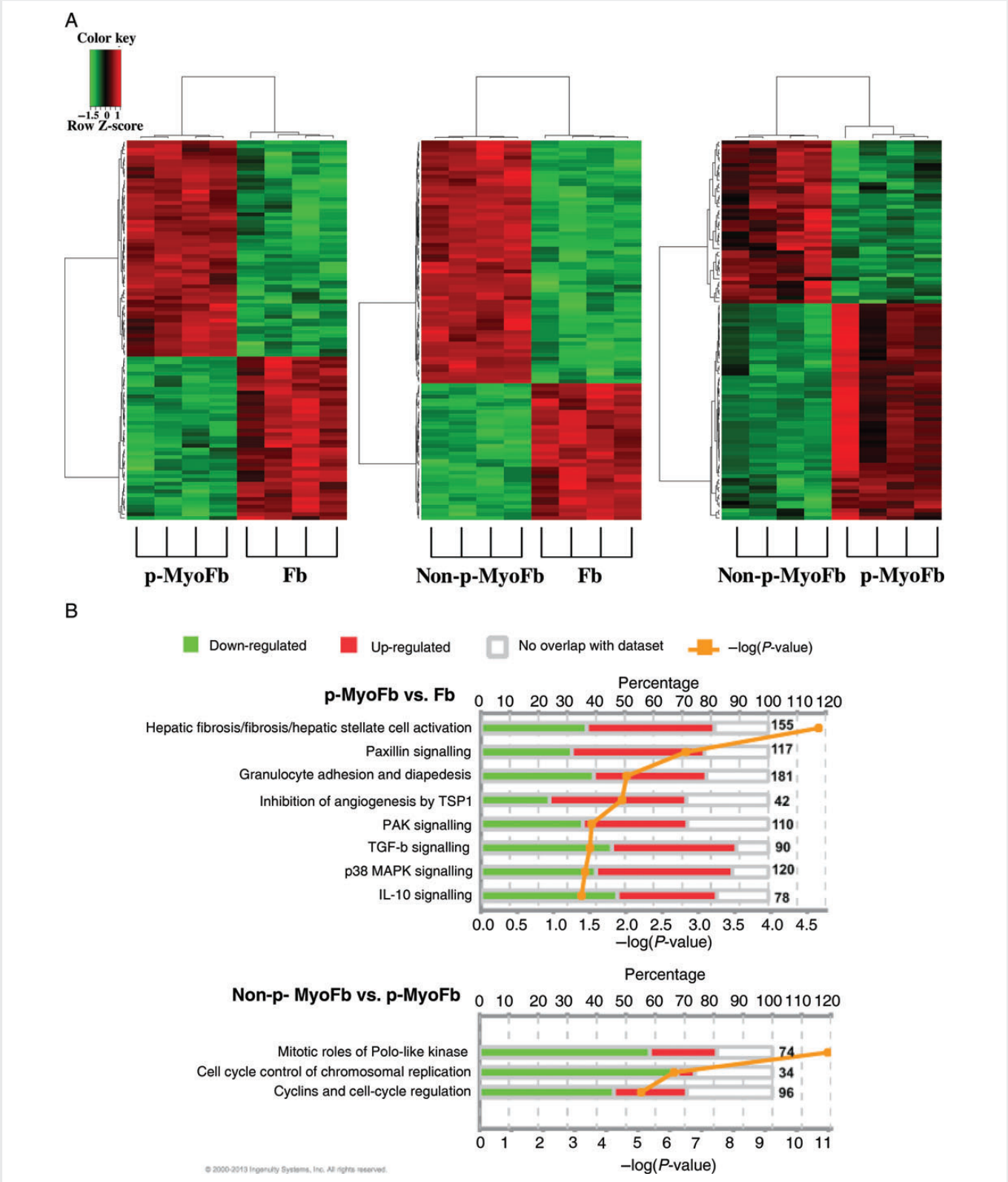

Figure 4 Differential gene expression in different Fb phenotypes. (*A*) Heat-maps showing distribution of the top 100 of differentially expressed genes ($P < 0.05$) between Fb, p-MyoFb, and non-p-MyoFb. (B) List of differentially regulated canonical pathways derived from the comparison between Fb, p-MyoFb, and non-p-MyoFb ($N = 4$). Bar graphs indicate the percentage of down-regulated (green) and up-regulated genes (red). The number of differentially expressed genes for each pathway is shown adjacent to the bar graph. Values higher than −log (*P*-value) of >1.3 indicate significant changed pathways (orange).

fibrosis', PAK signalling, paxilin signalling, TGF-beta signalling, p38 MAPK signalling, and IL-10 signalling (*Figure 4B*, top panel). Differential regulation of canonical pathways between p-MyoFb and non-p-MyoFb is restricted to cell proliferation including mitotic roles of Polo-like kinase, cell cycle control of chromosomal replication, and cyclins and cell cycle regulation pathways (*Figure 4B*, lower panel).

3.6 Blockade of TGF-β-RI signalling induces MyoFb dedifferentiation under mechanical stress

When differentiated p-MyoFb into 2-D cultures are treated for 4 days with SD-208 (*Figure 5A*,a and b), the number of cells with α-SMA-positive stress fibres (*Figure 5A*,c) decreases substantially compared with non-treated p-MyoFb (50 ± 7 vs. 74 ± 3%). Reduction of α-SMA staining occurs in cells of different sizes and is therefore probably not the result of new formed cells (see Supplementary material online, *Figure S5*). A fraction of p-MyoFb transforms to small-sized spread cells. Moreover, stress fibres and α-SMA are removed indicating p-MyoFb dedifferentiation (*Figure 5A*a and b). The other fraction has a similar cell size as p-MyoFb but shows loss of stress fibres. The presence of α-SMA aggregates in the cytoplasm suggests that p-MyoFbs are in an active dedifferentiation process (*Figure 5A*,b; insert). Morphological signs of apoptosis are not observed. De-polymerization of α-SMA-positive stress fibres is accompanied by a significant decrease in α-SMA protein expression (*Figure 5A*,d). ROCK inhibition in p-MyoFb with Y-27632 also shows a decrease in α-SMA protein levels.

Contrary to p-MyoFb, SD-208-treated non-p-MyoFb (*Figure 5B*,a and b) show only a minor decrease in the number of cells with α-SMA-positive stress fibres [(85 ± 4%; *Figure 5B*,c) compared with non-treated non-p-MyoFb (95 ± 2%)]. The majority of non-p-MyoFbs do not remove their stress fibres and α-SMA incorporation (*Figure 5B*a and b). Protein expression levels of α-SMA are not changed in either SD-208 or Y-27632 treated non-p-MyoFb (*Figure 5B*,d). These data indicate that TGF-β1 signalling blockade can induce MyoFb dedifferentiation even on a stiff substratum with mechanical stress. However, dedifferentiation is mainly restricted to p-MyoFb. Reversibility is a feature that discriminates p-MyoFb and non-p-MyoFb and indicates that the latter cells are terminally differentiated MyoFb.

3.7 Removal of mechanical tension in unrestrained collagen matrices induces MyoFb dedifferentiation

We examined whether loss of mechanical stress induced dedifferentiation of p-MyoFb and non-p-MyoFb by studying stress fibre and α-SMA integrity in unrestrained 3-DCMs, cultured without serum for 2 days. After 2 days of culture, a fraction of spread p-MyoFb (41%) shows G-actin aggregates (*Figure 6A*,a and g). This de-polymerization of stress fibres is associated with a release of bound α-SMA and its aggregation in the cytoplasm alongside G-actin (*Figure 6A*,c). Co-localization of G-actin aggregates and stress fibres is often observed suggesting stress fibre de-polymerization, which in some cells is very pronounced (*Figure 6A*,c). In a number of cells, stress fibres are completely de-polymerized showing only G-actin aggregates (*Figure 6A*,b). These observations point to the activation of a dedifferentiation process in p-MyoFb.

Non-p-MyoFbs are present as dendritic and elongated cells after 1 day of culture, with stress fibres decorated with α-SMA. 37% of stress fibre-positive cells show G-actin aggregates and α-SMA (*Figure 6A*,f and g). Co-localization of stress fibres and G-actin aggregates are often observed (*Figure 6A*,d and e). These data indicate that stress fibre de-polymerization is associated with G-actin and α-SMA release and their aggregation in the cytoplasm.

3.8 Further dedifferentiation of MyoFbs in the long-term culture

The data above suggest that p-MyoFb progressively dedifferentiate with time, while 60% of non-p-MyoFbs do not dedifferentiate at all after 2 days but a longer time frame is needed to support this interpretation. Non-restrained 3-DCM cultures cannot be continued longer because Fbs become apoptotic.[26] Long-term experiments are therefore performed in restrained 3-DCM, in which initial size is maintained, but without additional stretch, and with serum added to the medium. This condition is providing a more physiological environment. We predicted that if MyoFb dedifferentiation would start immediately after embedding, 3-DCM contraction and strain would remain mild and MyoFb dedifferentiation is further promoted. Indeed, *Figure 6B*,a and c shows that after 2 weeks in 3-DCM, 76% of p-MyoFbs are α-SMA negative indicating MyoFb dedifferentiation. In contrast, after incubation of non-p-MyoFb for 2 weeks in 3-DCM (*Figure 6B*,b and c), two cell fractions appear: (i) a majority of α-SMA-positive MyoFb (88% of cells) and (ii) a small fraction of α-SMA-negative cells. These data together with those obtained in 2-D cultures demonstrate the existence of two phenotypes of cardiac MyoFb with differences in reversibility of the phenotypes.

4. Discussion

4.1 Different phenotypes of cardiac Fb cells can be generated in cultures

Fbs derived from various organs show heterogeneity in size, morphology, proliferation, collagen secretion, and growth factors.[27,28] Heterogeneity in 2-D cultures can be explained, at least partly, by spontaneous differentiation into MyoFb, which are almost always residing in 2-D cultures.[12,16] Cultures of rat cardiac Fb have the absolute majority of MyoFb,[15] indicating that the Fbs are very labile cells and discrepancy between *in vitro* and *in vivo* studies of cardiac Fb is more pronounced than those for Fb of other origins. As a result, features of MyoFb may be non-specifically assigned to Fb. In the current study, we prevented spontaneous differentiation by inhibition of TGF-β1-RI kinase with SD-208, which blockades intracellular signalling downstream of TGF-β-RI as shown in pulmonary Fb.[29]

The transcriptome analysis showed a very rich set of differentially expressed genes. Networks that were differentially regulated between Fb and p-MyoFb relate to differentiation and are in agreement with the ultrastructural properties and functional characteristic differences between these cell types such as formation of focal adhesions and collagen production. Networks that are differentially regulated between p-MyoFb and non-p-MyoFb are in agreement with the differences in proliferation shown in the assay data. These gene expression profiles derived from the microarray analysis underscore and complement the functional and structural differences observed in our study.

4.2 Interaction between mechanical stress and TGF-β1 in Fb differentiation

The present data confirm that differentiation of isolated cardiac Fb to MyoFb on stiff substratum is entirely dependent on TGF-β1 signalling.

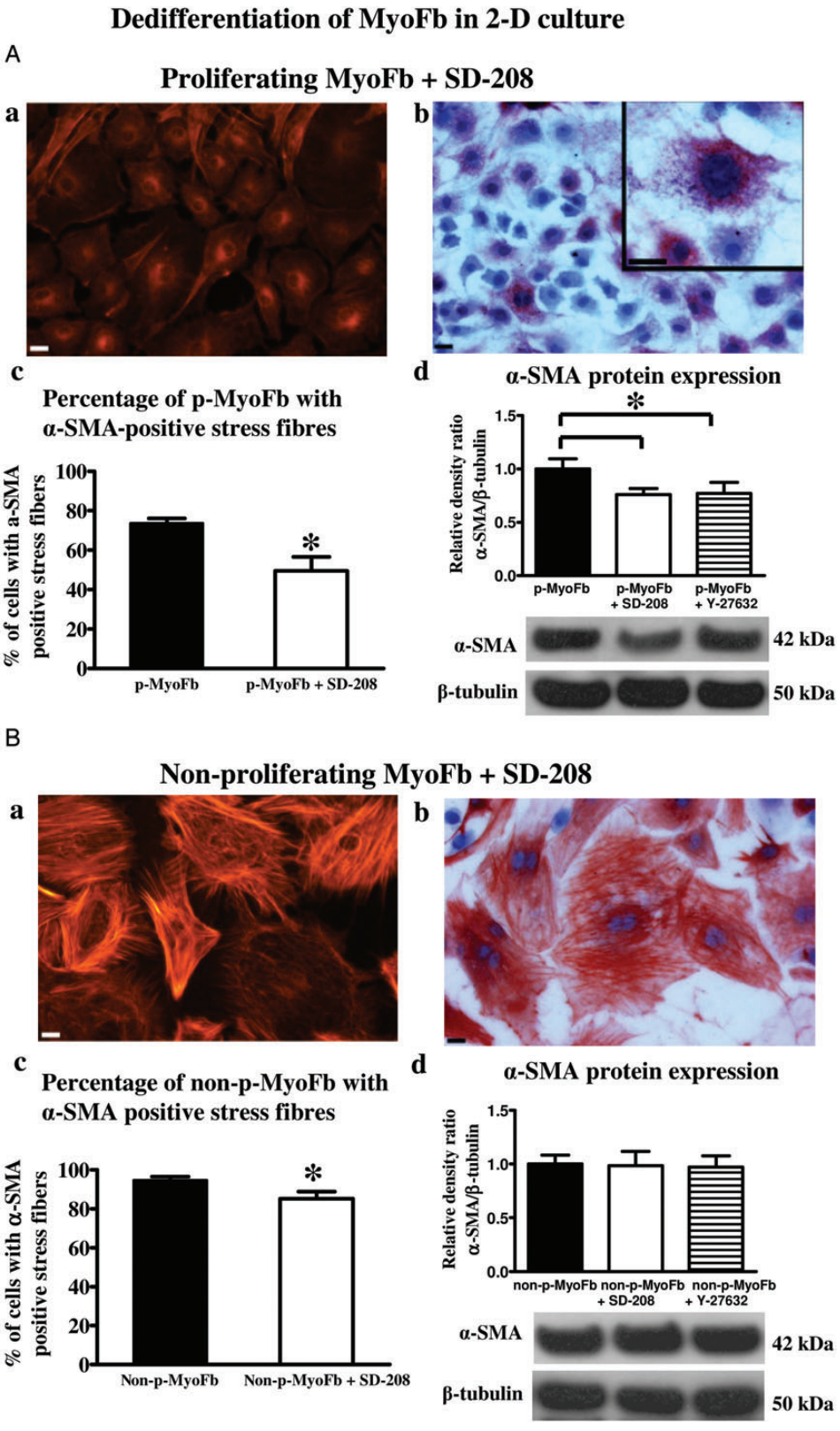

Figure 5 Effect of SD-208 on dedifferentiation of p-MyoFb and non-p-MyoFb in 2-D cultures. Treatments of p-MyoFb (*A*a–d) and non-p-MyoFb (*B*a–d) for 4 days with SD-208 (3 μmol/L). Cells are stained for stress fibres (*A*a and *B*a) and α-SMA (*A*b and *B*b); scale bars represent 20 μm. Insert in *A*b shows α-SMA cytosolic aggregates. (*A*c and *B*c) Quantification of cells with α-SMA-positive stress fibres. Western blotting of α-SMA in p-MyoFb (*A*d) and non-p-MyoFb (*B*d) treated with SD-208 during 4 days. *$P < 0.05$ vs. p-MyoFb or non-p-MyoFb ($N = 5$).

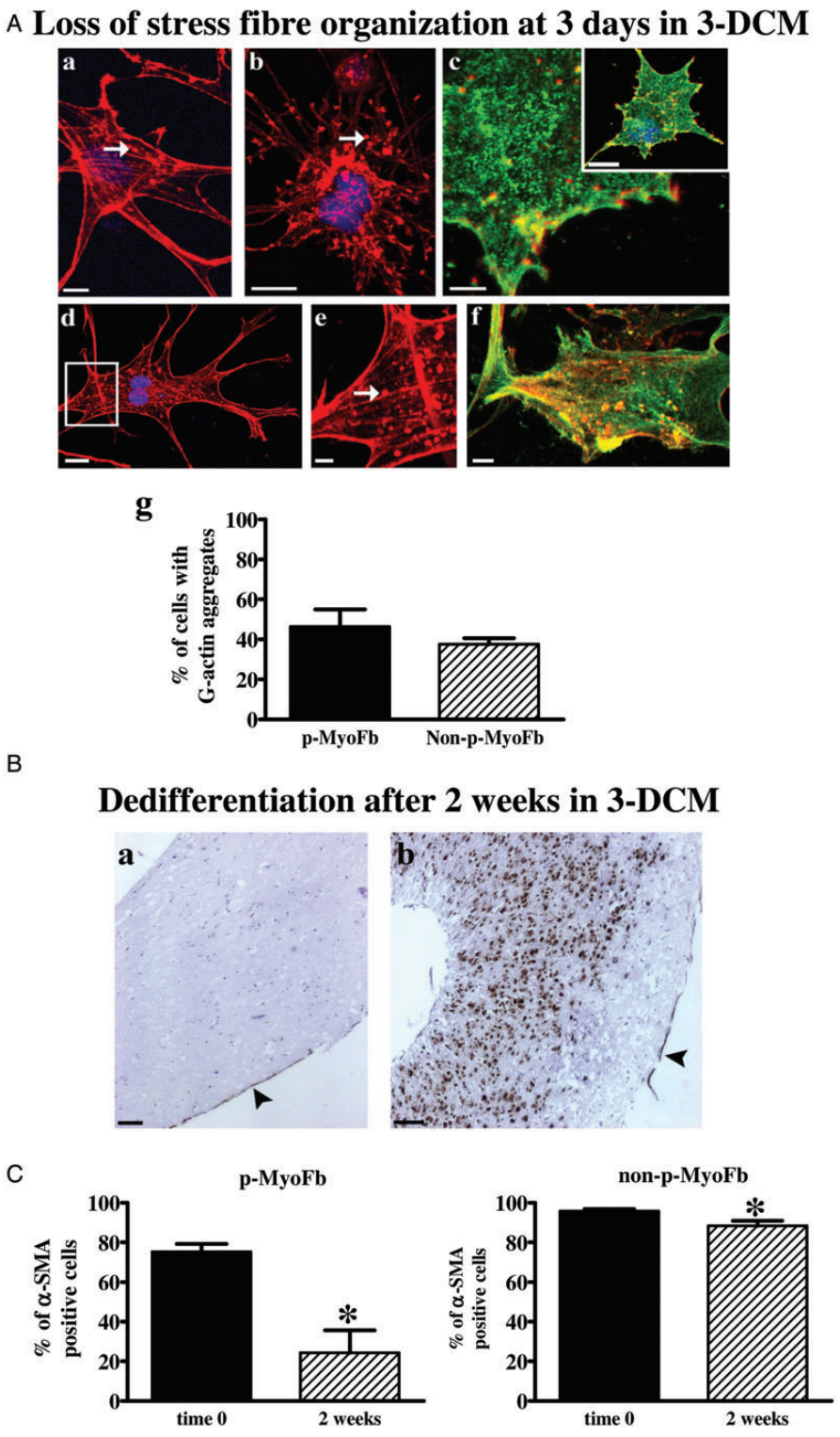

Figure 6 Dedifferentiation of p-MyoFb and non-p-MyoFb during cultures in 3-DCM. (*A*) Two-day cultures in unrestrained 3-DCM without serum; p-MyoFb (*Aa*–c) and non-p-MyoFb (*Ad*–f) double-labelled with Rhodamin-Phalloidin (red, *Aa*–f) and α-SMA antibodies (green, *Ac* and *Af*). Stress fibre de-polymerization in p-MyoFb into aggregates is marked in *Aa* and *Ab* by white arrows; α-SMA aggregates are observed in spread MyoFb (*Ac*; insert). (d–f) Non-p-MyoFbs also show stress fibre de-polymerization; magnification (*Ae*) of the stress fibre area (*Ad*; white rectangle) shows actin aggregates between stress fibres; *Af* shows α-SMA aggregates. (*Ag*) Quantification of p-MyoFb and non-p-MyoFb fractions with actin aggregates, mean ± SEM of three independent cultures. (*B*) Two-week cultures in restrained 3-DCM, p-MyoFb (*Ba*) and non-p-MyoFb (*Bb*) labelled for α-SMA (brown). Note the absence of α-SMA staining in p-MyoFb indicating dedifferentiation (edges are α-SMA positive, arrowheads). (*Bc*) Quantification of α-SMA-positive cells in restrained 3-DCM compared with 2-D cultures, mean ± SEM of five independent cultures. Scale bars represent 5 μm (*Ac* and *Ae*), 10 μm (*Aa*, *Af*); 20 μm (*Ab*, *Ac* insert, *Ad*), 100 μm (*Ba*), and 125 μm (*Bb*) .

TGF-β1 present at low levels in the serum may initiate the process and act as a direct stimulator of differentiation as supported by the effect of SD-208. Inhibition of ROCK, part of the TGF-β-signalling chain, attenuates Fb differentiation but not to the same extent as TGF-β-RI kinase blockade. Additional mechanisms such as focal adhesion maturation resulting from the mechanical stress, through TGF-β1, reinforce the process.[30] Thus, TGF-β-signalling has an important role in cell differentiation and stress fibre polymerization, both directly and through the translation of mechanical tension.

Moreover, TGF-β1 and ROCK increase the F-G-actin ratio, which promotes MRTF translocation to the nucleus and induces α-SMA expression.[9] Our data also indicate that MRTF-A is differentially regulated in Fb, p-MyoFb, and non-p-MyoFb. We show that high expression of MRTF-A in p-MyoFb is required for activation of MyoFb differentiation as reported previously.[9] Interestingly, we demonstrate that expression of MTRF-A is low in non-p-MyoFb. These data suggest that α-SMA expression in non-p-MyoFb is regulated via other signalling pathways. However, we were not able to investigate the translocation of the MRTF-A protein, which is thought to be critical for its function.

We further demonstrate that TGF-β1 is an important modulator of Fb function. Inhibition of TGF-β-RI signalling maintains low levels of collagen synthesis and prevents ECM contraction. Interestingly, we also find augmented secretion of IL-10 in the culture medium. IL-10 is an anti-inflammatory cytokine, which suppresses the production of inflammatory cytokines and has an anti-fibrotic effect on the heart.[31] Transcriptome analysis confirms a down-regulation of pathways responsible for Fb differentiation and fibrosis and a significant up-regulation of IL-10 signalling. We can therefore suggest that inhibition of TGF-β1 preserves the genuine Fb functional phenotype.

On the other hand, TGF-β1-induced differentiation of non-p-MyoFb is associated with increased secretion of inflammatory cytokines MCP-1 and TIMP-1. Previously, Westermann *et al.*[7] demonstrated up-regulation of TIMP-1 in TGF-β1 activated Fbs. TIMP-1 protects collagen through inhibition of MMPs and is found in high concentrations in cardiac scar tissue.[32] MCP-1 may reflect an important role of non-p-MyoFb in generating an inflammatory response via attraction of macrophages and in the development of fibrosis.[33] Functional parameters such as increased collagen synthesis, extracellular matrix contraction, and secretion of pro-fibrotic cytokines emphasize the role of non-p-MyoFb in adverse myocardial remodelling. p-MyoFb can functionally be distinguished from non-p-MyoFb due to their moderate involvement in collagen synthesis and ECM contraction. Differences in both MyoFb gene expression profiles are mainly attributed to pathways involved in cell proliferation. These data indicate that p-MyoFb and non-p-MyoFb are independent phenotypes, which differ at a functional and molecular level.

4.3 Loss of mechanical strain induces dedifferentiation of proliferating MyoFbs

Incorporation of 2-D cultured cells in 3-DCM shows that the Fb phenotype in 2-D cultures determines the initial phenotype in 3-D, at least in terms of the cytoskeleton. However, a significant number of MyoFb showed de-polymerization of stress fibres. Stress fibre assembly in spreading cells utilizes actin that already present in the cytoplasm, since protein synthesis inhibitors do not prevent stress fibre formation.[34] Therefore, the appearance of stress fibres depends only on G-actin polymerization/de-polymerization. This process is regulated by chaperones, such as αB crystalline and HSP27, which have actin as folding substratum and stabilize microfilaments.[35,36] It can be suggested that, without stimulation, chaperones that were induced in 2-D cultures could disappear with time in 3-D, inducing stress fibre de-polymerization.

Further loss of stress fibre organization and in particular of α-SMA indicate true dedifferentiation. Long-term culture in restrained (but non-stretched), 3-DCM led to profound dedifferentiation of p-MyoFb, indicating the primary role of mechanical stress to maintain differentiation. Low levels of TGF-β1 in the culture medium could not prevent this process. The observation that inhibition of TGF-β1 in 2D cultures, with maintained mechanical stress, could also induce dedifferentiation is consistent with a scheme in which TGF-β1 has a role in the translation of tension, as discussed above, and is not in contradiction with the central role for tension in maintaining differentiation. Moreover, preliminary data from our group show reduction of MRTF-A/B mRNA expression levels in p-MyoFb, but not in non-p-MyoFb after inhibition of TGF-β1. We suggest that de-polymerization of stress fibres during p-MyoFb dedifferentiation will decrease the F−G-actin ratio resulting in sequestration of MRTF-A/B and down-regulation of α-SMA expression.

Dedifferentiation was clear for p-MyoFb, but not for non-p-MyoFb. These data underscore the profound difference between two MyoFb phenotypes and indicate that non-p-MyoFbs are terminally differentiated cells. The existence of two MyoFb phenotypes explains the controversy of data reporting that MyoFbs are reversibly differentiated and others reporting that they are irreversibly differentiated.[37,38] Active dedifferentiation in p-MyoFb was shown for foetal lung Fb after deactivation of mitogen-activated protein kinase and MyoD.[14] Both p- and non-p-MyoFb are present in the myocardium after myocardial infarction. p-MyoFbs appear temporarily, shortly after infarction,[39] while non-p-MyoFb appear at the latest steps of healing where they persist for years in the scar tissue.[40] Apoptosis mediates the disappearance of p-MyoFb during the transition of granulation tissue to scar tissue.[39] Our data could provide another mechanism for the disappearance of p-MyoFb, i.e. MyoFb dedifferentiation.

5. Conclusions

Cardiac fibroblastic cells have a high degree of plasticity with a continuum of phenotypes from true Fb to non-p-MyoFb. Mechanical strain and growth factors are interdependently involved in differentiation and dedifferentiation. Blocking TGF-β-RI kinase or reduction of mechanical strain promotes p-MyoFb dedifferentiation, while non-p-MyoFb do not dedifferentiate indicating that non-p-MyoFb have reached a steady-state phenotype which is insensitive to changes in mechanical load and TGF-β1. Strategies for the treatment of extracellular matrix remodelling should thus preferably target (de)differentiation of proliferating MyoFbs.

Supplementary material

Supplementary material is available at *Cardiovascular Research* online.

Acknowledgements

Microarray analysis was performed by the VIB Nucleomics Core (KU Leuven, www.nucleomics.be) and further support was provided by the Genomics Core facility (KU Leuven) for the protein array analysis.

Conflict of interest: The authors declare that there is no conflict of interest.

Funding

This work was supported by the Research Foundation Flanders (FWO-Vlaanderen, postdoctoral Fellowship, R.D.) and by the Belgian Science Policy Program P6/31 (K.S.). Funding to pay the Open Access publication charges for this article was provided by the Research Foundation Flanders (FWO-Vlaanderen, postdoctoral Fellowship, R.D.).

References

1. Krenning G, Zeisberg EM, Kalluri R. The origin of fibroblasts and mechanism of cardiac fibrosis. *J Cell Physiol* 2010;**225**:631–637.
2. Dobaczewski M, Gonzalez-Quesada C, Frangogiannis NG. The extracellular matrix as a modulator of the inflammatory and reparative response following myocardial infarction. *J Mol Cell Cardiol* 2010;**48**:504–511.
3. Hinz B, Mastrangelo D, Iselin CE, Chaponnier C, Gabbiani G. Mechanical tension controls granulation tissue contractile activity and myofibroblast differentiation. *Am J Pathol* 2001;**159**:1009–1020.
4. Bowers SLK, Banerjee I, Baudino TA. The extracellular matrix: at the center of it all. *J Mol Cell Cardiol* 2010;**48**:474–482.
5. Sun Y, Weber KT. Infarct scar: a dynamic tissue. *Cardiovasc Res* 2000;**46**:250–256.
6. Petrov VV, Fagard RH, Lijnen PJ. Transforming growth factor-β1 induces angiotensin-converting enzyme synthesis in rat cardiac fibroblasts during their differentiation to myofibroblasts. *J Renin Angiotensin Aldosterone Syst* 2000;**1**:342–352.
7. Westermann D, Lindner D, Kasner M, Zietsch C, Savvatis K, Escher F *et al*. Cardiac inflammation contributes to changes in the extracellular matrix in patients with heart failure and normal ejection fraction. *Circ Heart Fail* 2011;**4**:44–52.
8. Tomasek JJ, Gabbiani G, Hinz B, Chaponnier C, Brown RA. Myofibroblasts and mechano-regulation of connecting tissue remodeling. *Nat Rev Mol Cell Biol* 2007;**3**:349–363.
9. Small EM, Thatcher JE, Sutherland LB, Kinoshita H, Gerard RD, Richardson JA *et al*. Myocardin-related transcription factor-a controls myofibroblast activation and fibrosis in response to myocardial infarction. *Circ Res* 2010;**107**:294–304.
10. Wang J, Chen H, Seth A, McCulloch CA. Mechanical force regulation of myofibroblast differentiation in cardiac fibroblasts. *Am J Physiol* 2003;**285**:H1871–H1881.
11. Khouw IM, van Wachem PB, Plantinga JA, Vujaskovic Z, Wissink MJ, de Leij LF *et al*. TGF-β and bFGF affect the differentiation of proliferating porcine fibroblasts into myofibroblasts in vitro. *Biomaterials* 1999;**20**:1815–1822.
12. Rohr S. Cardiac fibroblasts in cell culture systems: myofibroblasts all along? *J Cardiovasc Pharmacol* 2011;**57**:389–399.
13. Asker SF, Bingen BO, Swildens J, Ypey DL, van der Laarse A, Atsma DE *et al*. Connexin43 silencing in myofibroblasts prevents arrhythmias in myocardial cultures: role of maximal diastolic potential. *Cardiovasc Res* 2012;**93**:434–444.
14. Hecker L, Jagirdar R, Jin T, Thannickal VJ. Reversible differentiation of myofibroblasts by MyoD. *Exp Cell Res* 2011;**317**:1914–1921.
15. Artaud-Macari E, Goven D, Brayer S, Hamimi A, Besnard V, Marchal-Somme J *et al*. Nuclear factor erythroid 2-related factor 2 nuclear translocation induces myofibroblastic dedifferentiation in idiopathic pulmonary fibrosis. *Antioxid Redox Signal* 2012; .
16. Hinz B, Gabbiani G, Chaponnier C. The NH_2-terminal peptide of α-smooth muscle actin inhibits force generation by the myofibroblast in vitro and in vivo. *J Cell Biol* 2002;**13**:657–663.
17. Rosker C, Salvarani N, Schmutz S, Grand T, Rohr S. Abolishing myofibroblast arrhythmogeneicity by pharmacological ablation of α-smooth muscle actin containing stress fibers. *Circ Res* 2011;**109**:1120–1131.
18. Dobaczewski M, Bujak M, Li N, Gonzalez-Quesada C, Mendoza LH, Wang XF *et al*. Smad3 signaling critically regulates fibroblast phenotype and function in healing myocardial infarction. *Circ Res* 2010;**107**:418–428.
19. Petrov VV, van Pelt JF, Vermeesch JR, Van Duppen V, Vekemans K, Fagard RH *et al*. TGF-β1-induced cardiac myofibroblasts are nonproliferating functional cells carrying DNA damages. *Exp Cell Res* 2008;**314**:1480–1494.
20. Desmouliere A, Geinoz A, Gabbiani F, Gabbiani G. Transforming growth factor-β1 induces α-smooth muscle actin expression in granulation tissue myofibroblasts and in quiescent and growing cultured fibroblasts. *J Cell Biol* 1993;**122**:103–111.
21. Zhao XH, Laschinger C, Arora P, Szaszi K, Kapus A, McCulloch CA. Force activates smooth muscle α-actin promoter activity through the Rho signaling pathway. *J Cell Sci* 2007;**120**:1801–1809.
22. Vardouli L, Moustakas A, Stournas C. LIM-kinase 2 and cofilin phosphorylation mediate actin cytoskeleton reorganization induced by transforming growth factor-β. *J Biol Chem* 2005;**280**:11448–11457.
23. Ehrlich HP, Rittenberg T. Differences in the mechanism for high- versus moderate-density fibroblast-populated collagen lattice contraction. *J Cell Physiol* 2000;**185**:432–439.
24. Petrov VV, Fagard RH, Lijnen PJ. Stimulation of collagen production by transforming growth factor-beta1 during differentiation of cardiac fibroblasts to myofibroblasts. *Hypertension* 2002;**39**:258–263.
25. Porter KE, Turner NA. Cardiac fibroblasts: at the heart of myocardial remodeling. *Pharmacol Ther* 2009;**123**:255–278.
26. Niland S, Cremer A, Fluck J, Eble JA, Krieg T, Sollberg S. Contraction-dependent apoptosis of normal dermal fibroblasts. *J Invest Dermatol* 2001;**116**:686–692.
27. Fries KM, Blieden T, Looney RJ, Sempowski GD, Silvera MR, Willis RA *et al*. Evidence of fibroblast heterogeneity and the role of fibroblast subpopulations in fibrosis. *Clin Immunol Immunopathol* 1994;**72**:283–292.
28. Smith TJ, Sempowski GD, Wang HS, Del Vecchio PJ, Lippe SD, Phipps RP. Evidence for cellular heterogeneity in primary cultures of human orbital fibroblasts. *J Clin Endocrinol Metab* 1995;**80**:2620–2625.
29. Kapoun AM, Gaspar NJ, Wang Y, Damm D, Liu YW, O'Young G *et al*. Transforming growth factor-β receptor type 1 (TGFβRI) kinase activity but not p38 activation is required for TGFβRI-induced myofibroblast differentiation and profibrotic gene expression. *Mol Pharmacol* 2006;**70**:518–531.
30. Goffin JM, Pittet P, Csucs G, Lussi JW, Meister JJ, Hinz B. Focal adhesion size controls tension-dependent recruitment of alpha-smooth muscle actin to stress fibers. *J Cell Biol* 2006;**172**:259–268.
31. Krishnamurthy P, Rajasingh J, Lambers E, Qin G, Losordo DW, Kishore R. IL-10 inhibits inflammation and attenuates left ventricular remodeling after myocardial infarction via activation of STAT3 and suppression of HuR. *Circ Res* 2009;**104**:e9–e18.
32. Heymans S, Schroen B, Vermeersch P, Milting H, Gao F, Kassner A *et al*. Increased cardiac expression of tissue inhibitor of metalloproteinase-1 and tissue inhibitor of metalloproteinase-2 is related to cardiac fibrosis and dysfunction in the chronic pressure-overloaded human heart. *Circulation* 2005;**112**:1136–1144.
33. Frangogiannis NG, Dewald O, Xia Y, Ren G, Haudek S, Leucker T *et al*. Critical role of monocyte chemoattractant protein-1/CC chemokine ligand 2 in the pathogenesis of ischemic cardiomyopathy. *Circulation* 2007;**115**:584–592.
34. Goldman RD, Knipe KP. Functions of cytoplasmic fibers in nonmuscle cell motility. *Cold Spring Harbor Simp Quant Biol* 1973;**37**:5231–5534.
35. Ghosh JG, Houck SA, Clark JI. Interactive sequences in the stress protein and molecular chaperone human alphaB crystallin recognize and modulate the assembly of filaments. *Int J Biochem Cell Biol* 2007;**39**:1804–1815.
36. Hirano S, Shelden EA, Gilmont RR. HSP27 regulates fibroblast adhesion, motility, and matrix contraction. *Cell Stress Chaperones* 2004;**9**:29–37.
37. Evans RA, Tian YC, Steadman R, Phillips AO. TGF-β1-mediated fibroblast-myofibroblast terminal differentiation-the role of Smad proteins. *Exp Cell Res* 2003;**282**:90–100.
38. Maltseva O, Folger P, Zekaria D, Petridou S, Masur SK. Fibroblast growth factor reversal of the corneal myofibroblast phenotype. *Invest Ophthalmol Vis Sci* 2001;**42**:2490–2495.
39. Desmouliere A, Redard M, Darby I, Gabbiani G. Apoptosis mediates the decrease in cellularity during the transition between granulation tissue and scar. *Am J Pathol* 1995;**146**:56–66.
40. Willems IE, Havenith MG, De Mey JG, Daemen MJ. The α-smooth muscle actin-positive cells in healing human myocardial scars. *Am J Pathol* 1994;**145**:868–875.